A laboratory based system for Laue micro x-ray diffraction

P. A. Lynch,[a] A. W. Stevenson, D. Liang, D. Parry, and S. Wilkins
Commonwealth Scientific and Industrial Research Organization, Manufacturing and Infrastructure Technology, Private Bag 33, Clayton South MDC, 3169, Australia

N. Tamura
Advanced Light Source, Lawrence Berkeley National Laboratory, 1 Cyclotron Road, Berkeley, California 94720

(Received 25 April 2006; accepted 8 January 2007; published online 9 February 2007)

A laboratory diffraction system capable of illuminating individual grains in a polycrystalline matrix is described. Using a microfocus x-ray source equipped with a tungsten anode and prefigured monocapillary optic, a micro-x-ray diffraction system with a 10 μm beam was developed. The beam profile generated by the ellipsoidal capillary was determined using the "knife edge" approach. Measurement of the capillary performance, indicated a beam divergence of 14 mrad and a useable energy bandpass from 5.5 to 19 keV. Utilizing the polychromatic nature of the incident x-ray beam and application of the Laue indexing software package X-Ray Micro-Diffraction Analysis Software, the orientation and deviatoric strain of single grains in a polycrystalline material can be studied. To highlight the system potential the grain orientation and strain distribution of individual grains in a polycrystalline magnesium alloy (Mg 0.2 wt % Nd) was mapped before and after tensile loading. A basal (0002) orientation was identified in the as-rolled annealed alloy; after tensile loading some grains were observed to undergo an orientation change of 30° with respect to (0002). The applied uniaxial load was measured as an increase in the deviatoric tensile strain parallel to the load axis.
 [DOI: 10.1063/1.2437777]

I. INTRODUCTION

Historically, the potential of the Laue method has been restricted to single crystal and large grain crystal structures. Such restrictions are the result of limited flux in laboratory x-ray sources and the complex nature of experimental Laue patterns arising from polycrystalline materials. Using the continuous spectrum of high brilliance synchrotron sources, precision focusing optics, along with the availability of high speed computers, the potential of the Laue method has been rediscovered in recent years. For example, Laue micro-x-ray diffraction (μXRD) has been used to study the orientation,[1] residual stress,[2] and defect concentration[3,4] within individual grains of polycrystalline materials. With focused spot sizes less than 100 nm reported,[5] μXRD shows potential for solving problems presently encountered in existing microscopy techniques. For example, TEM studies of heavily deformed Mg alloys are problematic due to contrast overlap caused by large concentrations of dislocations and twinning defects. Similar problems have also been observed in electron backscattering diffraction studies.[6]

Although synchrotron beamlines lead the development of future μXRD experimentation, an inherent problem which is particularly apparent in this field is the increasing demand and limited availability of synchrotron-based μXRD resources. Utilizing modern x-ray source and optics development, laboratory μXRD instrumentation and experimentation is an area of growing interest. In recent years, the successful application of laboratory μXRD instrumentation has led to the availability of commercial systems with a spatial resolution ranging from 50 to 300 μm.[7]

Microbeam formation processes rely on the ability to efficiently image or demagnify the x-ray source onto the sample. Various formation techniques have been proposed and one of the most successful methods, based on mirror focusing, was pioneered in the 1950s.[8] More recently, other focusing mechanisms have been studied by many researchers. Some of these optic designs include zone plates,[9,10] single/poly capillaries,[11] microchannel plates,[12] and compound refractive lenses.[13] Although many focusing optics exist, each approach is intrinsically linked to the properties of the x-ray source and focus requirements, consequently most focusing methods are application specific.[14] For example, white beam μXRD requires a focusing optic with high spatial resolution and broad energy bandpass; Kirkpatrick-Baez mirrors and capillary optics have traditionally been used to meet these demands.[11]

Capillary focusing is one area of x-ray optics research that has undergone considerable development, especially for the generation of microbeams using laboratory x-ray sources. Several competing factors must be satisfied to achieve an optimal capillary design. These include the focused beam size requirements, beam divergence, and x-ray source.[15] The physical basis underpinning capillary design is the total external reflection of x rays from a smooth surface.[16] Consequently material and surface roughness properties play a leading role in describing the optic performance. Typically glass capillary optics are preferred due to their high β/δ

[a]Electronic mail: Peter.Lynch@csiro.au

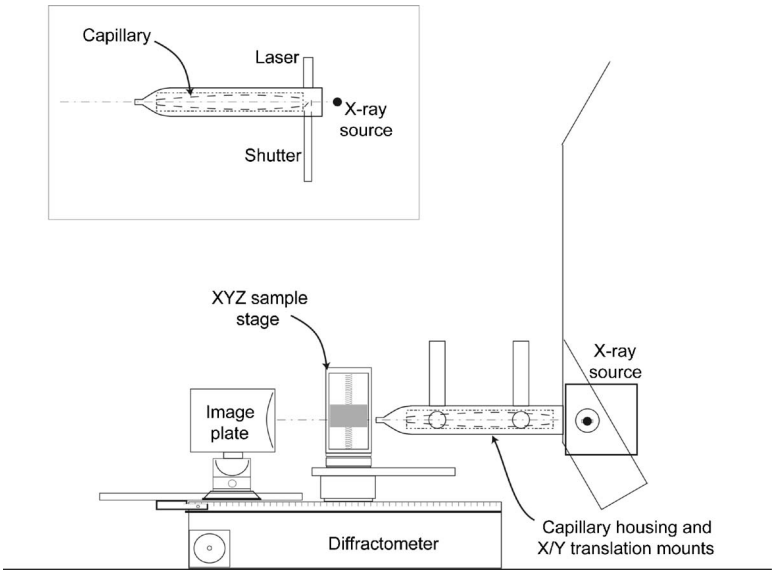

FIG. 1. Schematic illustration showing the design and geometry of the laboratory μXRD system. The inset provides a detailed view of the capillary housing and shutter/mirror system with respect to the laser used for sample alignment.

ratio, where β represents the imaginary absorption component and δ the real dispersion component of the complex refractive index. One of the first demonstrations of fiber technology as applied to capillary optics was reported by Rindby (1986),[17] the relationship between x-ray energy and observed x-ray deviation in a pyrex glass fiber was quantified by measurement of the critical angle for total reflection. Using a straight capillary design, beam sizes down to about 10 μm were achieved from standard x-ray tubes.[18]

Subsequent optic design has utilized drawing processes to manufacture prefigured geometries that exhibit superior performance characteristics. Some of these shapes include; tapered/conical,[19,20] parabolic,[21] and ellipsoidal.[22] A common feature of these prefigured optics is their condensing type nature, i.e., photons entering the capillary bore undergo total external reflection along the optic length until they emerge from the exit bore. This can be problematic because the inner wall surface roughness plays a major role in terms of the transmission efficiency. Moreover, a reduction in the beam size introduces increased beam divergence which places significant restrictions on the sample positioning to achieve maximum flux from the optic. It is found that the transmission efficiency of capillary devices can be drastically improved by reducing the number of reflections a photon must undergo.[23] Improvements in this area have been reported through the development of single bounce optics; it has been demonstrated that a paraboloidal prefigured capillary is capable of producing a transmission efficiency of ~90% with the focal plane well beyond the exit aperture.[15] Most recently, it has been highlighted that as a result of the improvements initiated by prefigured optics, the major gain is presently achieved by minimizing the slope deviation from the ideal guiding figure.[14]

Quality prefigured optics coupled with high brilliance microfocus x-ray sources have displayed considerable promise in laboratory applications. In general, monocapillary and polycapillary optics are used for diffraction and fluorescence measurements, respectively. Using a parabolic optic and custom built x-ray generator Yamamoto [24] designed a laboratory instrument with a spatial resolution of 0.8 μm. X-ray fluorescence (XRF) and diffraction spectra were used to study the microstructural properties of high performance ultra-large-scale integrated devices. Using a laboratory μXRF spectrometer equipped with a capillary optic, Wegrzynek[25] conducted a feasibility study highlighting the capabilities of absorption based computer microtomography imaging. Case studies were carried out on various samples and a spatial resolution of a few tens of micrometers was reported. Based on a modular design, Bjeoumikhov *et al.*[26] used a commercial low-power microfocus source with various polycapillary optics to perform μXRF and μXRD. For the diffraction experiments absorbing foils were introduced in order to obtain a reasonable degree of monochromaticity in the primary beam. One of the underlying features apparent in the laboratory-based μXRD literature is that although the studies highlighted the natural polychromatic bandpass of the capillary, diffraction experiments were confined to the high-intensity characteristic lines of the incident beam/source.

In the present contribution a laboratory system that utilizes the background continuum radiation to collect polychromatic Laue data is reviewed. Measurements have been performed to address the properties of the incident beam profile and performance of the capillary optic. Finally, application of the laboratory μXRD system to study the individual grain orientation and deviatoric strain in a polycrystalline magnesium alloy MgNd (magnesium 99.98%, Nd 0.2%) is demonstrated.

II. MICRODIFFRACTION SYSTEM

The x-ray microdiffraction system developed in this work is illustrated in Fig. 1. The specific microstructural information that can be studied with this instrumentation is highly sample dependent, in particular, grain size dependent. In the first instance, where the grain size is less than the focused x-ray spot size, crystal structure information relating to the phase, grain (domain) size, and macroscopic deformation (stress/strain) relationships can be achieved. Alternately, when the sample grain size is of similar dimensions or greater than the incident x-ray beam, grain specific informa-

tion can be realized. Accordingly, the instrumentation design has been optimized for the latter case, i.e., Laue μXRD studies. As illustrated in Fig. 1, a laboratory based μXRD system requires several key hardware components, including; a microfocus x-ray source, focusing capillary x-ray optic, high-resolution sample mapping stage and area detection system.

The objective in designing the source and preoptic configuration illustrated in Fig. 1 was to maximize the number of photons incident upon the sample within the desired spot size without introducing excessive beam divergence. Accordingly, it was possible to produce a 10 μm x-ray spot by using a commercially available microfocus x-ray source (Feinfocus) equipped with a W anode and a focusing capillary x-ray optic (AXCO). Based on the resources available for calculating the efficiency of a 10 μm focal spot for μXRD applications, the underpinning system features were the source brightness and capillary gain/efficiency.

For the present application, the x-ray source figure of merit is brightness which is directly related to the maximum power density, and therefore the minimum beam diameter of the incident electron beam which can be delivered to the target anode without causing damage. Using the steady state heat flow equation, Grider *et al.*[27] presented a method for measuring the electron beam radius and hence x-ray source radius in a microfocus tube as a function of the electron beam power corresponding to the onset of target damage. For three different target materials, a linear dependence was observed between the source size and applied power. As an approximate guide, the source size scaled according to the applied power in a 1:1 ratio, i.e., for each watt of power the source size increases by ~ 1 μm^2. For the present microfocus x-ray source, based on the manufacturer's guidelines, the operating conditions range from 0–160 kV with an anode current of 0–3 mA. Experiments were undertaken to determine the optimum source operating conditions. Although dependent upon the efficiency of the capillary optic and x-ray source power limits, the experimental settings used in this study were 30 kV and 1–3 mA, a maximum power of 90 W, with a corresponding source size ranging from 30 to 90 μm^2.

A focusing capillary optic supplied by AXCO[28] was manufactured according to the x-ray source size, focus properties, and spectral transmission requirements. To optimize the capillary gain and efficiency, the ability to model the transmission efficiency according to profile shape[23] and to accurately fabricate a predefined capillary profile was essential; this task was conducted by AXCO. Using their novel fabrication technique an ellipsoidal shaped optic 110 mm long, with a theoretical focal spot size of 10 μm and gain of 180$\times$ was manufactured for the μXRD system.

The inset of Fig. 1 shows a schematic illustration of the capillary design with reference to the source position. Several key manufacturing features were essential for this design, including location of the capillary entrance aperture 12 mm away from the source, this enabled the standard Be window on the source to remain in place. The optic was also fixed within two brass cylinders, the smaller diameter cylinder positioning the optic while the larger diameter provides mechanical strength and support for Oriel DC Mike motors needed to automate X and Y translations near the entry and exit bore of the capillary. Moreover, this design acts as a form of shielding, minimizing background leakage caused by high energy x rays penetrating through the capillary walls. At the capillary focal plane an aperture was added to restrict the component of the direct beam passing through the capillary without undergoing reflection. Although the intensity of this component of the direct beam is small compared to the focused spot, the aperture was justified as it reduces the intensity in the tail of the incident spot distribution.[15] Furthermore, the aperture also blocks incident x rays that may have undergone transmission through the capillary walls.

To accurately align the sample and to perform localized area mapping studies, a high-resolution XYZ stage was mounted on the diffractometer axis of rotation. Positioning the specimen region of interest with respect to the x-ray focus was achieved by the introduction of a laser beam onto the sample surface along a coaxis of the x-ray beam, as shown in Fig. 1. To collect the diffraction data high-resolution image plates (200 mm$\times$250 mm, 25 μm pixel size) were positioned on a slide rail mounted on the 2θ arm of the diffractometer. For indexation purposes it was essential to provide an accurate and reproducible method for positioning the image plate with respect to the incident beam. This aspect was resolved by manufacturing an image plate holder which incorporated a series of apertures for precise relocation after processing. Moreover, due to the physical size of the image plate it was possible to record the position of the direct beam which was also used as a further reference point.

A. Characteristics of the incident x-ray beam

1. Optic alignment

Capillary alignment was automated by Oriel X and Y translation drives mounted perpendicularly to the beam propagation direction at the entrance and exit of the capillary. Observation of the beam issuing from the capillary was achieved by imaging the focused spot using a charge-coupled device (CCD) detector placed approximately 50 mm from the focal plane. When the capillary was suitably aligned an intense spot surrounded by an annulus of comparable intensity was observed (Fig. 2). The annulus could be moved with small translations of the capillary tip, however the central spot remained stationary during these translations. From these observations it was concluded that the central spot consisted of x-rays that had not been reflected by the capillary walls and was emanating directly from the source. The surrounding annulus corresponded to x rays undergoing total external reflection from the capillary walls, diverging past the focal plane.

In an attempt to provide a quantitative method for the optic alignment a scintillation detector with a pulse height discriminator set at various energy levels (Cu $K\alpha$, Mo $K\alpha$) was used to measure the observed count rate as a function of the capillary translation position. Although this approach provided a measure of the incident intensity, this was problematic because it was necessary to attenuate the direct beam with Al filters, resulting in beam hardening. Bearing this in

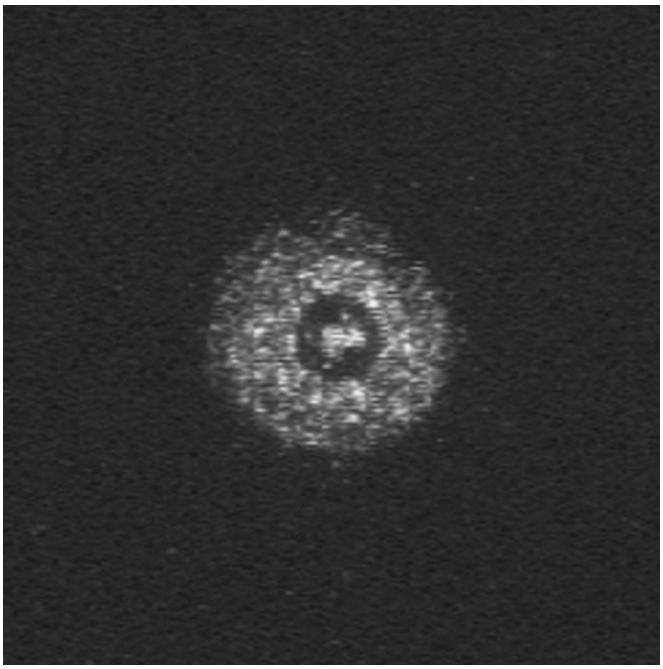

FIG. 2. CCD image recorded at a distance of ~50 mm from the end of the exit aperture of the optic, showing the central spot surrounded by a uniform annular ring due to x-rays undergoing total external reflection from the capillary walls.

mind it was possible to minimize this effect by recording the output energy spectrum of the incident beam using an energy dispersive Si(Li) detector.

2. X-ray focus

Once the x-ray throughput of the optic was maximized, the size and profile of the emerging beam was determined using the knife edge method.[19] To perform this task a piece of tantalum with a highly polished edge was mounted parallel to the face of the aperture on the high-resolution *XYZ* translation stage. A scintillation detector set for Cu $K\alpha$ and Mo $K\alpha$, positioned 50 mm from the aperture, was used to monitor the observed incident beam intensity as the knife edge was translated laterally through the beam issuing from the capillary. Stepping in 1.0 μm increments enabled one to estimate the beam size in the horizontal and vertical directions, Fig. 3(a) highlights this result for translation of the knife edge in the horizontal (X) direction. The rate of change of the observed intensity with respect to the knife edge position was calculated and the full width at half maximum (FWHM) intensity found. Figure 3(b) shows this differential data and the calculated FWHM obtained from fitting a Gaussian function to the data; in this instance the fitted FWHM was 9.2 μm. In performing subsequent analysis, the fitted Gaussian function of the differential data was highly dependent on the initial and final slope of the knife edge data, illustrated in Fig. 3(a), corresponding to no interception of and then totally blocking the beam, respectively. As a result the FWHM could only be used as an approximate measure of the beam size emanating from the capillary. Independent of this discrepancy, the result confirms that the beam was confined within the capillary bore and exit defining aperture. Furthermore, this confirms the present source/optic configuration produces a 10 μm incident beam.

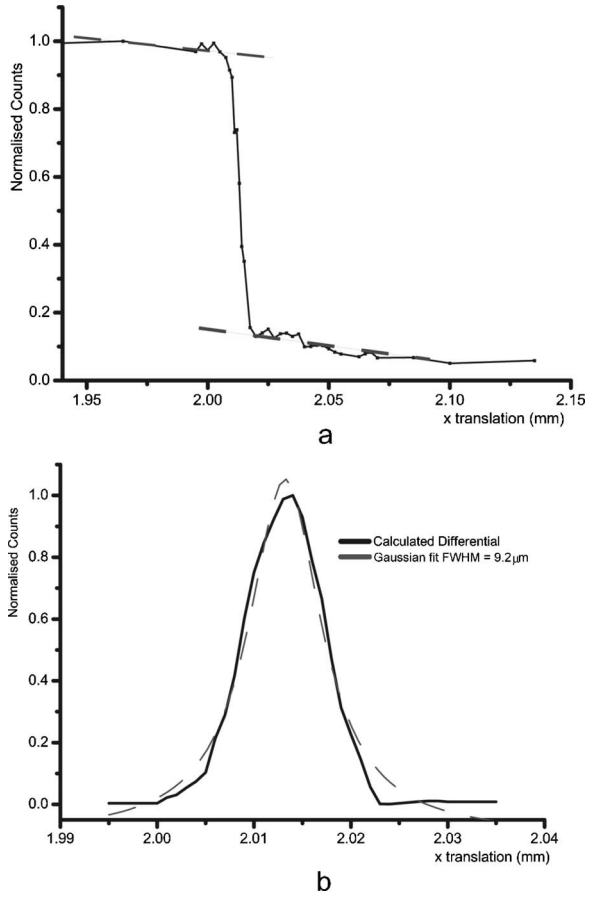

FIG. 3. Knife edge test of the beam emerging from the capillary/aperture. Data were collected using a scintillation detector with the pulse height discriminator set at 8.04 keV. (a) Data collected as the knife edge undergoes x-translation. (b) Differential data of the knife edge experiment and corresponding Gaussian fit with a FWHM=9.2 μm.

3. Beam divergence and optic gain

Two parameters intrinsically linked to the performance of a focusing capillary are the beam divergence and optic gain. In other words, the increased x-ray flux at the focal plane achieved with the optic must be considered in terms of the level of collimation necessary to satisfy the experimental requirements. For example, an area of intended research that will be undertaken using the present instrumentation is the analysis of smearing in Laue patterns arising from grain deformation. As the FWHM measure of the Laue spot will be utilized, it is necessary to ensure broadening arising from beam divergence is negligible compared to deformation induced smearing. Consequently, to achieve a practical focal spot of 10 μm, a divergence of ~10–15 mrad is considered adequate for the majority of applications.

To quantify the experimental broadening in the measured Laue data arising from beam divergence, it was necessary to collect a Laue pattern from a strain-free Si single crystal. Employing a diverging reflection geometry[29] with the sample at the beam focus and image plate beyond the focus at a distance of 150 mm, a measure of the divergence could be ascertained. A portion of the collected data is shown in Fig. 4. In this case the broadening associated with the measured Laue spot is the convolution of the incident beam spot size, x-ray source energy distribution, beam divergence, and mo-

FIG. 4. Laue data from a Si (111) single crystal collected at a sample to image plate distance of 150 mm, the inset shows a diffraction spot at 3× magnification.

saic spread of the crystal. Assuming divergence is the dominant effect, from measurement of the spot size and with knowledge of the image plate distance from the sample, the experimentally determined divergence was found to be 14 mrad which is in reasonable agreement with the theoretical divergence of 12 mrad.

For the present experimental setup the gain in x-ray flux at the focal plane realized with the focusing capillary optic was measured. The optic performance was determined by recording the integrated intensity at the focal plane with the capillary in position, compared to the recorded integrated intensity for a 20 μm aperture at the same distance from the source. Furthermore, to verify the measured capillary performance against the theoretically calculated gain for a single bounce ellipsoidal optic, several different source conditions were examined. Both the theoretical and experimentally measured optic gains are summarized in Table I.

The experimental results are in approximate agreement with theoretically calculated gain values for each source power loading. As an energy dispersive detector was not available to perform the gain measurements the difference between experimental and theoretical results may be due to the energy response of the image plates used to record the spot intensity. This is in agreement with experimental studies of an image plate pixel value response to the x-ray beam energy spectrum.[30] Furthermore, as a x-ray shutter was not installed on the system a small error may arise in the experimental results due to slight timing discrepancies. Both the theoretical and experimental values highlight the impact of the source size (power loading) on the optic collection efficiency, i.e., as the power loading is increased the source size expands well beyond the 6 mrad collection solid angle of the capillary entrance resulting in a substantial gain decrease. Finally, as the experimental gain is a maximum (73%) at 30 kV, 1 mA with respect to the theoretical result this is evidence the fabricated ellipsoidal optic shape is in close agreement with the initial theoretical design specifications based on a 30 μm^2 x-ray source.

TABLE I. Theoretical and experimental optic gain for a 20 μm focused spot at four source power settings.

Applied voltage (kVp)	Applied current (mA)	Theoretical gain	Experimental gain
30	1.00	700	507
30	1.66	400	273
30	2.33	270	176
30	3.00	180	114

4. Energy spectrum

The most challenging requirement of Laue diffraction on a laboratory level is to maximize the low-intensity continuum spectrum. In this instance, a x-ray tube with a high atomic number (Z) anode material is seen as a considerable advantage, since the continuum radiation is proportional to (Z). For example, due to the difference in atomic number between the elements Cu and W, the observed white radiation from the W tube will be ~2.5× more than a Cu tube operated at the same power. With this gain in intensity a W anode was essential for the present application. Another consideration in regard to the source was the applied power, as both the characteristic and continuum spectrum scale with applied power it was necessary to maximize this operating condition. However, as discussed in Sec. II the source size is also load dependent. Therefore, a compromise had to be made between the maximum intensity and minimum source size so the most effective collection efficiency of the optic could be realized. It was then necessary to test the ideal source settings with the optic in place. After several studies 30 kV and 1–3 mA appeared to suit the optic/source combination, which equates to a source size of ~30–90 μm.

The inherent characteristics of the capillary further assisted in obtaining a polychromatic bandpass for Laue diffraction experiments. That is, a focusing type capillary is designed with an incoming acceptance angle, within which incident photons of a given energy undergo total external reflection at the capillary walls and are focused at a point beyond the exit aperture. For the ellipsoidal capillary the acceptance angle was designed for an x-ray energy cutoff of

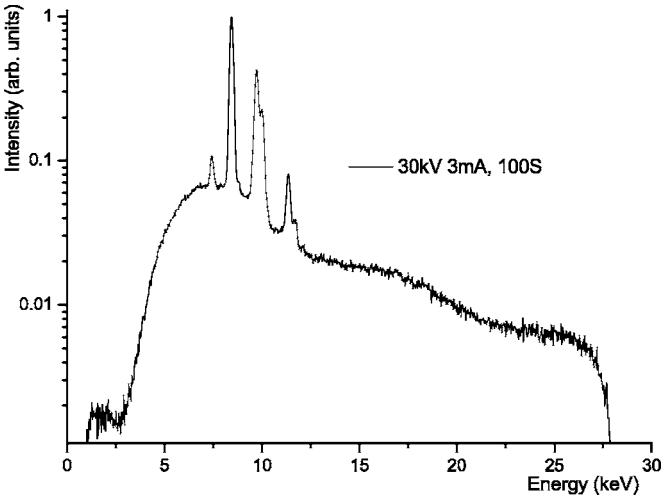

FIG. 5. Energy dispersive spectrum of the focused x-ray spot emerging from the capillary.

22 keV. Therefore, ignoring efficiency losses, all x rays entering the capillary with an energy less than 22 keV that undergo total external reflection will emanate from the capillary at the focus.

To measure the observed energy bandpass incident on the sample, an energy dispersive detector was placed 50 mm from the exit aperture of the capillary. The observed energy spectrum from the focused spot is given in Fig. 5. The recorded data was collected for 100 s with a source accelerating voltage of 30 kV and current of 3 mA. Although the aim was to maximize the white radiation, due to the applied voltage (30 kV) the intensity of the characteristic W $L\alpha$ and W $L\gamma$ lines shown in Fig. 5 are significantly higher than the continuum maximum. From observation of the energy bandpass emanating from the capillary and from indexing the diffraction pattern arising from the Si reference material, outlined in Sec. II B, the useable energy bandpass of the capillary was from 5.5 to 19 keV.

It should be noted that the presence of characteristic and continuum components of the x-ray spectrum in the focused spot can be easily identified in the collected diffraction pattern. For example, when a specimen displays a random orientation with grain size equivalent and/or greater than the focused spot size, the probability of obtaining diffraction from a characteristic line is low and consequently the Laue patterns arise from the continuum spectrum. Conversely when a polycrystalline sample exhibits a grain size significantly smaller than the spot size a Debye Scherrer ring pattern is observed, since the probability of many small crystallites obeying the Bragg diffraction condition corresponding to the energy of the characteristic radiation is significantly increased. Therefore, the analysis procedure is highly dependent upon the specimen's grain size.

B. Instrument calibration

In terms of the instrumental requirements, one of the main prerequisites for crystal structure determination is precise knowledge of the instrument geometry. Instrument calibration represents the first step toward the successful indexation of a measured Laue pattern and subsequent analysis. Calibration was performed by collecting data from an "ideal" strain free single crystal sample; for this task a Si (111) single crystal was used. The recorded reference pattern, given in Fig. 6, was obtained using a symmetric reflection geometry with the sample (ω) angle at 20°, image-plate angle (2θ) centered at 40°, at a distance of 45 mm from the sample. For these experiments image plates were preferred due to their high x-ray sensitivity and the associated low intensity of the diffraction pattern. Diffraction patterns were also collected with a CCD detector and these preliminary CCD measurements will be discussed in Sec. IV.

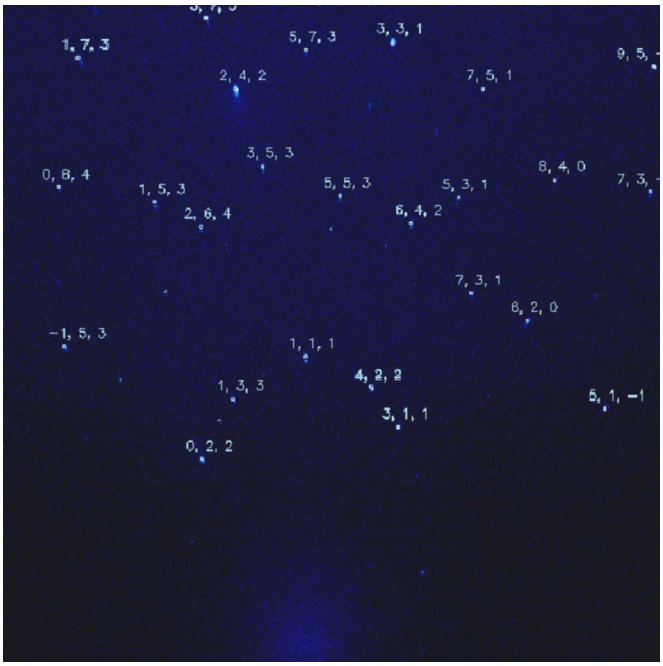

FIG. 6. Measured diffraction pattern from Si (111) single crystal reference material. Data collected at 30 kV, 3 mA with an exposure time of 45 min. White boxes and corresponding Miller indices represent the fit achieved for the experimental data.

For indexation of the Si single-crystal pattern and experimental patterns arising from the polycrystalline samples the μXRD software package X-Ray Micro-Diffraction Analysis Software (XMAS) (Refs. 31 and 32) was employed; for further details the reader is referred to Ref. 33. Prior to indexation, the known experimental conditions are required as input for the XMAS indexation package and these parameters include: the image-plate window size (100 mm × 70 mm); the ω and 2θ angles of 20° and 40°, respectively; energy bandpass of the tungsten source ~5.5 to 19 keV; an estimate of the sample-to-detector distance (dd ~45 mm) and the center position of the image plate (detector) in the x direction (Xcent) and y direction (Ycent), which were initially set to Xcent=350 and Ycent=500.

After successfully indexing the Si reference pattern, further refinement of the geometrical parameters dd, (Xcent), (Ycent) can be achieved by the method of triangulation.[34] After recording several Si reference patterns by varying the distance between the specimen and image plate in 5 mm increments (i.e., dd=45,50,...,70 mm triangulation can be used to determine a more accurate measure of the distance

TABLE II. Refined instrumental calibration parameters obtained from indexation of the Si reference material.

ω ($^\circ\theta$)	2θ ($^\circ 2\theta$)	X_{cent}	Y_{cent}	dd (mm)	$X\gamma$ ($^\circ$)	$X\beta$ ($^\circ$)
20	40	920.5	730.5	46	−0.75	−0.2

dd for the closest recorded pattern (dd=45 mm together with the (*X*cent) and (*Y*cent) values for this pattern. After updating these parameters, final calibration of the instrumental parameters including the detector tilt and rotation angles *Xalfd*, *Xbetd* , and *Xgam* can be refined for the reference material. These final calibrated parameters are listed in Table II. The final indexation result for the Si reference pattern, obtained with these settings, is illustrated in Fig. 6. Indexed Laue spots in the collected data are signaled by a white box with associated Miller indices. Ensuring the instrument geometry is unchanged the geometric settings given in Table II are incorporated as instrument input parameters for indexation of samples with unknown orientation.

III. OBSERVATION OF GRAIN ORIENTATION AND LATTICE STRAIN IN MgNd

To highlight the system capability to track the orientation and strain of individual grains in a polycrystalline material, diffraction measurements were collected from a cast Mg-Nd (99.98% Mg, 0.2% Nd) alloy sample. The cast Mg alloy was prepared by hot rolling to a thickness of 1 mm. After a post-rolling anneal the sample was polished to provide an estimate of the average grain size (Fig. 7). From optical microscopy measurements grains were found to be approximately equiaxed with a size varying from 10 μm to ~100 μm.

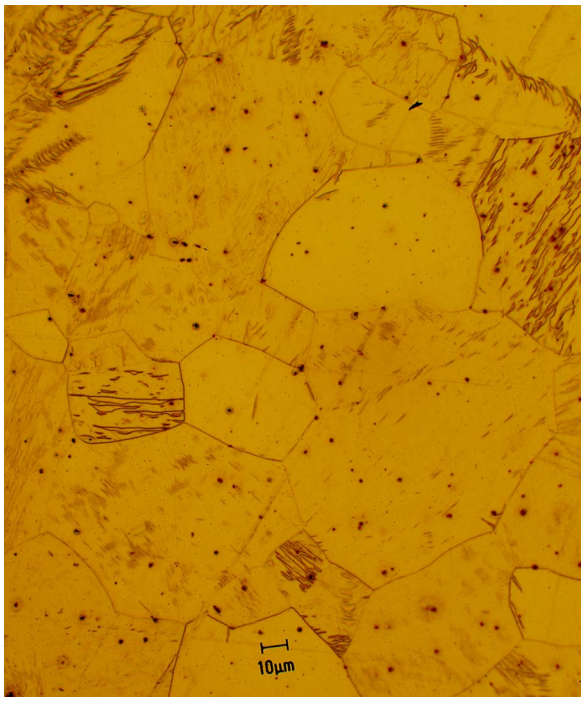

FIG. 7. Optical microscope image of the polished Mg-Nd sample providing an indication of the average grain size, magnification ×50.

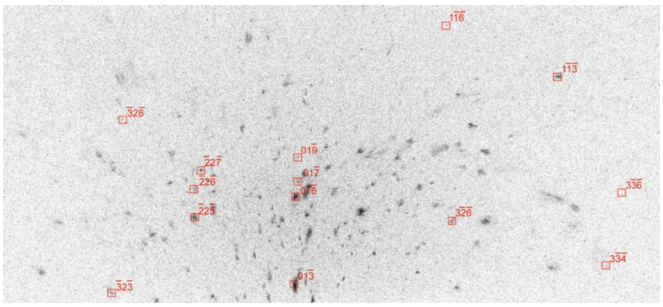

FIG. 8. Experimental diffraction pattern from the annealed Mg-Nd sample, exposure time 1 h. Squares and Miller indices represent indexation of the "'highest integrated intensity" grain.

For the present study two sets of μXRD measurements were collected; the first set was recorded for the annealed sample while the second set was collected after the specimen had undergone uniaxial tensile loading to an engineering strain of 2.5%. All data collection was undertaken using the same experimental geometry as employed for the Si reference material. That is, symmetric reflection with the sample angle ω=20°, 2θ=40° and the refined sample-to-detector distance dd=46 mm. To provide a measure of the change in orientation and strain of neighboring grains the scanning μXRD approach was used.[35] In this mode, the sample is raster scanned (20 μm steps) under the focused x-ray beam. For each step increment a diffraction pattern was recorded, in total a 100 μm line scan was collected before and after tensile loading. For the W x-ray energy spectrum emanating from the capillary optic, at 10 keV the attenuation length of Mg is ~300 μm. As a result it was anticipated that each recorded diffraction pattern would represent an illumination of 10–15 grains. An example of the recorded data for the annealed sample is given in Fig. 8. From the complex "spotted" diffraction pattern it is clearly evident that the grain size is greater than or of similar size to the incident beam size.

Due to the complexity of the measured patterns only grains indexed with at least 15 diffraction spots were considered. Based on this criteria it was possible to determine the orientation matrix of about ten grains in each experimental pattern. It should be noted with image-plate data collection, time requirements made it prohibitive to perform triangulation to resolve depth information of the diffracting grains. It is anticipated the efficiency of this aspect of the work will be greatly improved by incorporating a CCD detector, an area of future development for the present system. Consequently, the results presented are based on the indexed grain from each image which displays the highest integrated intensity. For example, indexation of the diffraction spots from a single grain, each spot highlighted by a white box with associated Miller indices, for the annealed specimen is illustrated in Fig. 8.

Utilizing the refined orientation matrices for each of the "highest integrated intensity" grains, the out-of-plane and in-plane orientations were calculated. Results for the line scan data are illustrated in Fig. 9 for the Mg-Nd sample before and after tensile loading. Figures 9(a) and 9(c) show the relative change in the angle between the [0002] direction and surface normal for each grain before and after tensile loading

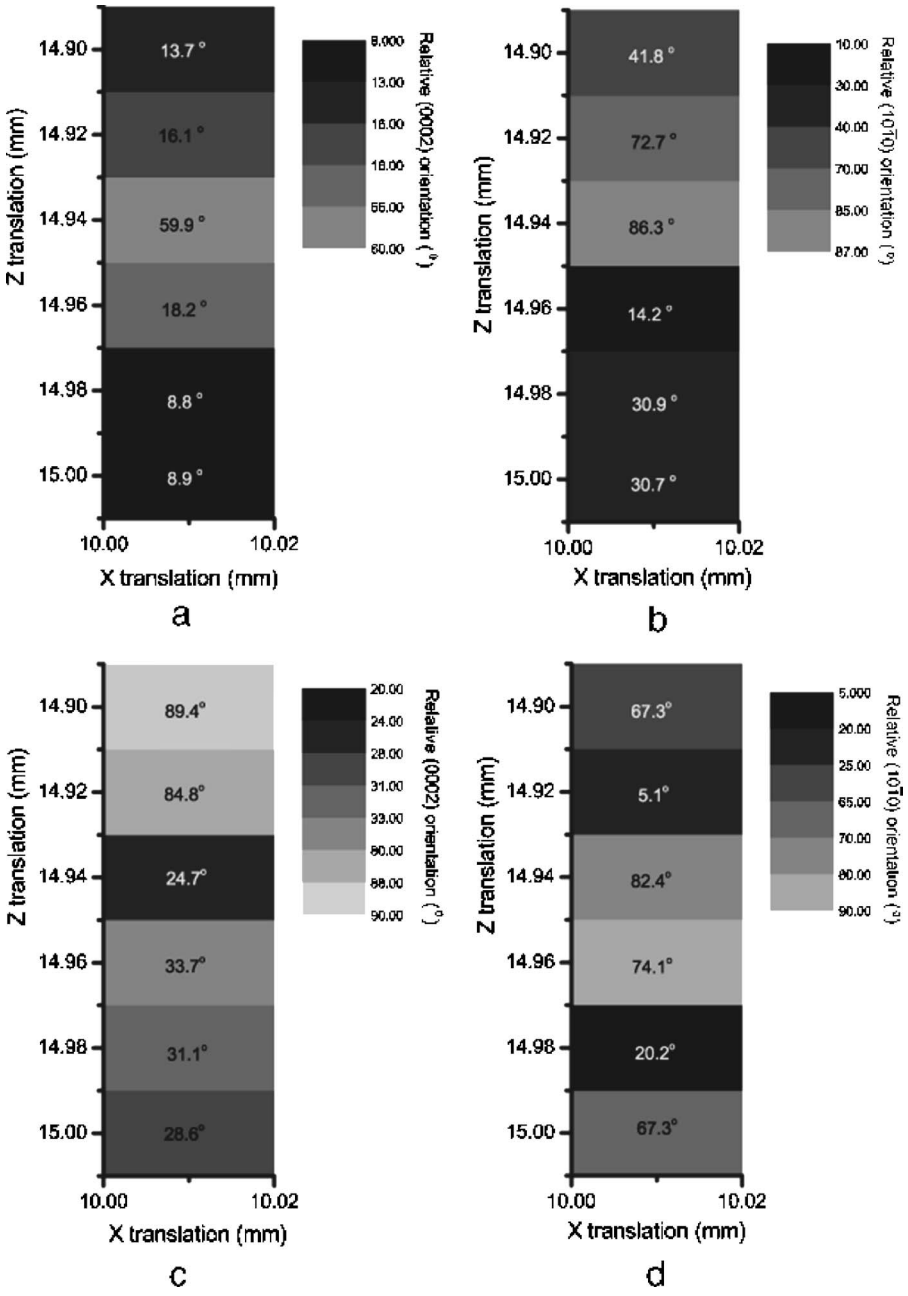

FIG. 9. Out-of-plane and in-plane (tensile axis) orientation from indexed grains that exhibit the highest integrated intensity from the line scan data of the annealed (a), (b) and tensile deformed (c), (d) Mg-Nd sample. (a),(c) Out-of-plane orientation relative to (0002), (b), (d) In-plane orientation relative to (10$\bar{1}$0), parallel to the tensile axis.

respectively. Figures 9(b) and 9(d) show the relative change in the angle between the [10$\bar{1}$0] direction and the in-plane sample x direction (tensile axis) for each grain before and after tensile loading, respectively. In the annealed state the majority of Mg-Nd grains display a basal orientation with a random in-plane orientation, a texture commonly encountered in bulk measurement studies from rolled Mg alloys.[36,37] An indication of the grain size can also be ascertained from the sample scanning approach. For the Z stage positions of 14.98 and 15.00 mm the out-of-plane and in-plane orientations are practically equal [Figs. 9(a) and 9(b)]. This signifies diffraction from the same grain at least 40 μm in size. In principle, the resolution of the grain size measurement is dictated by the step size.

For the loaded sample some of the grains in the initial basal texture appear to undergo an orientation change of 30° with respect to [0002], initiated by plastic deformation at a load of 2.5% strain. Since the sample had to be removed to perform tensile loading it was not possible to locate the same grain set to make a direct comparison, hence relative changes discussed in this study are restricted to grains from a similar region in the sample. Independent of this, further studies are presently being undertaken to determine the microstructural significance of the observed orientation change. In conjunction with the observed orientation change the induced plastic deformation also produced streaking (broadening) and splitting of the diffraction spots. These effects are caused by dislocation slip promoting grain sub-division. This is in agreement with the collected line scans showing unique grains for each step increment. This aspect of the work, determining the twin type and/or slip mechanisms is currently in progress.

An additional feature of the diffraction measurements is the ability to measure the induced lattice strain (d-spacing)

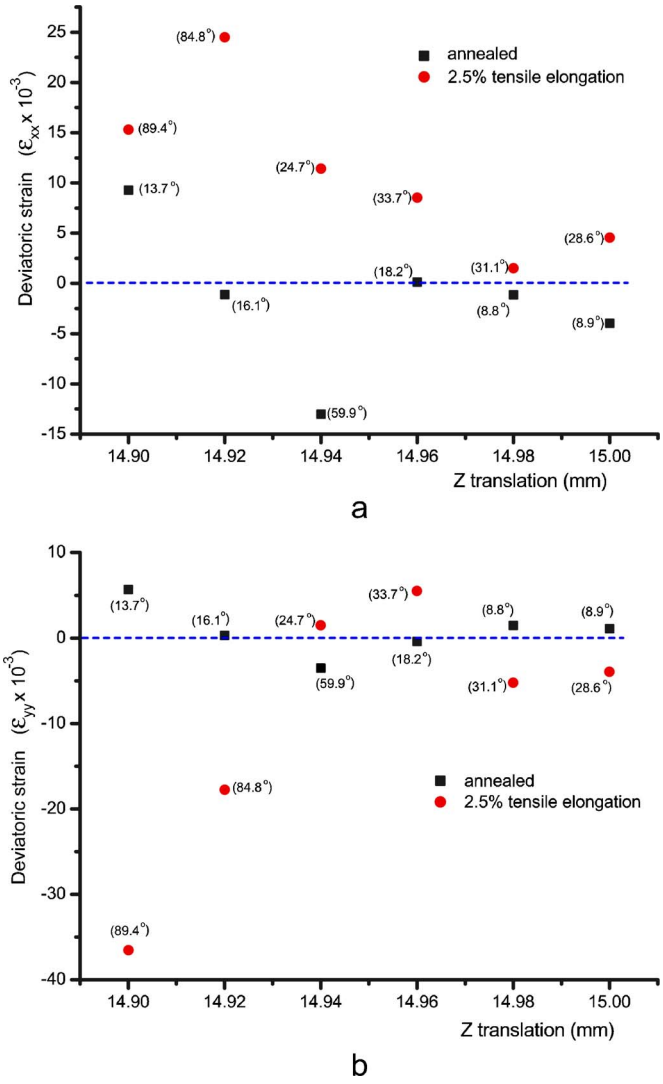

FIG. 10. Relative in-plane strain observed in the highest integrated intensity grains before and after an applied strain of 2.5%. (a) Normal strain component parallel to the elongation axis. (b) Normal strain component perpendicular to the elongation axis. Values in brackets indicate out-of-plane orientation with respect to (0002).

based on the observed spot positions relative to the "strain free" state. Expressed in tensor notation the measured strain can be specified for a given sample direction. The results for the in-plane strain components (ε_{XX} and ε_{YY}) for the line scan data are illustrated in Fig. 10. As mentioned, it was not possible to make a direct comparison between grains before and after loading and so relative lattice strain shifts are based on an average effect. Prior to deformation, the points for the in-plane strain, in the tensile direction ε_{XX} and transverse direction ε_{YY} are approximately zero, a result consistent with the post rolling anneal. After tensile loading, the majority of grains exhibit a tensile strain parallel to the load axis and compressive component perpendicular to the tensile axis.

IV. DISCUSSION

As demonstrated for the MgNd alloy, the microdiffraction system and subsequent data processing was used to determine the orientation matrix and strain tensor of individual grains in a bulk matrix before and after load application. The ability to measure this microstructural information at an individual grain level should provide useful input and verification for the next generation of deformation models. For example, the ability to track the orientation of individual grains provides a precise method for determining twinning mechanisms as a function of applied load. Moreover, the ability to quantify individual grain structure information from a laboratory instrument serves as a highly useful preliminary data set if further high-resolution μXRD studies are to be performed at a synchrotron facility.

To improve the statistical relevance of the measured individual grain data, an increased population of grains must be characterized. This is an area which demands further instrument development. Having proven that the weakly scattering diffraction pattern can be adequately collected using image plates, a primary focus of continued instrument development lies in the area of data collection automation. For the samples studied in this report preliminary measurements have been carried out with an uncooled CCD detector. Even with the poor dark current characteristics of the present CCD it was possible to collect diffraction patterns within ~30 min. Further work is planned using a cooled CCD with an increased active area size. The addition of data collection automation will greatly assist in the ability to track a greater ensemble of grains and will also improve triangulation methods to establish the scattering depth of individual grains.

V. CONCLUSION

By utilizing the small spot size capabilities of a microfocus x-ray source coupled with the flux gain achieved with a single bounce capillary optic, a laboratory microdiffraction system with a spatial resolution of 10 μm was realized. In conjunction with the high-spatial resolution, the continuous nature of the x-ray (polychromatic) spectrum of the tungsten source enabled diffraction measurements to be performed without requiring sample rotation. Indexation of the experimental diffraction pattern arising from individual grains in a bulk polycrystalline Mg-Nd alloy was achieved with the software package XMAS. Using a raster scan approach and with subsequent analysis, for the majority of grains, a general basal (0002) grain orientation was observed in the post roll annealed Mg-Nd sample. After tensile loading to an engineering strain of 2.5%, the individual grain texture appeared to undergo an orientation change of 30° with respect to (0002). The applied strain was quantified as an in-plane tensile and compressive strain parallel and perpendicular to the load axis respectively.

ACKNOWLEDGMENTS

The authors would like to thank K. Venkatesan for preparing and performing the strain test on the MgNd sample, C. Bettles and M. Gibson for scientific discussions and encouragement throughout the development of this project. This work was supported by the Victorian Centre for Advanced Materials Manufacturing (VCAMM).

[1] G. C. Butler, S. R. Stock, R. D. McGinty, and D. L. McDowell, J. Eng. Mater. Technol. **124**, 48 (2002).
[2] J. S. Chung and G. E. Ice, J. Appl. Phys. **86**, 5249 (1999).

[3] R. Barabash, G. E. Ice, B. C. Larson, G. M. Pharr, K.-S. Chung, and W. Yang, Appl. Phys. Lett. **79**, 749 (2001).
[4] R. I. Barabash, G. E. Ice, B. C. Larson, and W. Yang, Rev. Sci. Instrum. **73**, 1652 (2002).
[5] O. Hignette, P. Cloetens, G. Rostaing, P. Bernard, and C. Morawe, Rev. Sci. Instrum. **76**, 063709 (2005).
[6] M. R. Barnett, M. D. Nave, and C. J. Bettles, Mater. Sci. Eng., A **386**, 205 (2004).
[7] B. A. GMBH Technical Report (Bruker AXS, Inc., 1998).
[8] P. Kirkpatrick and A. V. Baez, J. Opt. Soc. Am. **38**, 756 (1948).
[9] E. D. Fabrizio, F. Ramanato, M. Gentili, S. Cabrini, B. Kaulich, J. Susini, and R. Barnett, Nature (London) **9**, 895–898 (1999).
[10] M. Altissimo, F. Romanato, L. Vaccari, L. Businaro, D. Cojoc, B. Kaulich, S. Cabrini, and E. D. Fabrizio, Microelectron. Eng. **61–62**, 173 (2002).
[11] D. H. Bilderback, S. A. Hoffman, and D. J. Thiel, Science **263**, 201 (1994).
[12] S. Wilkins, A. W. Stevenson, K. A. Nugent, H. Chapman, and S. Steenstrup, Rev. Sci. Instrum. **60**, 1026 (1989).
[13] A. Snigirev, V. Kohn, I. Snigirev, and B. Lengeler, Nature **384**, 49 (1996).
[14] D. H. Bilderback, X-Ray Spectrom. **32**, 195 (2003).
[15] D. X. Balaic, K. Nugent, Z. Barnea, R. Garrett,and S. Wilkins, J. Synchrotron Radiat. **2**, 296 (1995).
[16] A. H. Compton and S. K. Allison, *X-Rrays inTheory and Experiment* (Van Nostrand, New York, 1935).
[17] A. Rindby, Nucl. Instrum. Methods Phys. Res. A **249**, 536 (1986).
[18] D. A. Carpenter, X-Ray Spectrom. **18**, 253 (1989).
[19] D. J. Thiel, D. H. Bilderback, A. Lewis, E. A. Stern, and T. Rich, Appl. Opt. **31**, 987 (1992).
[20] P. Engstrom, S. Larsson, A. Rindby, A. Buttkewitz, S. Garbe, G. Gaul, A. Knochel, and F. Lechtenberg, Nucl. Instrum. Methods Phys. Res. A **302**, 547 (1991).
[21] N. Yamamoto and Y. Hosokawa, Jpn. J. Appl. Phys., Part 2 **27**, L2203 (1988).
[22] A. Attaelmanan, P. Voglis, A. Rindby, S. Larsson, and P. Engstrom, Rev. Sci. Instrum. **66**, 24 (1995).
[23] D. X. Balaic and K. A. Nugent, Appl. Opt. **34**, 7263 (1995).
[24] N. Yamamoto, Rev. Sci. Instrum. **67**, 3051 (1996).
[25] D. Węgrzynek, X-Ray Spectrom. **30**, 413 (2001).
[26] A. Bjeoumikhov, N. Langhoff, J. Rabe, and R. Wedell, X-Ray Spectrom. **33**, 312 (2004).
[27] D. E. Grider, A. Wright, and P. K. Ausburn, J. Phys. D **19**, 2281 (1986).
[28] D. X. Balaic, Australian X-ray Capillary Optics Pty Ltd. (AXCO). http://axco.com.au
[29] D. X. Balaic, Z. Barnea, K. A. Nugent, R. F. Garrett, J. N. Varghese, and S. Wilkins, J. Synchrotron Radiat. **3**, 289 (1996).
[30] D. M. Tucker, P. S. Rezentes, and A. Assoc, Phys. Med. **24**, 887 (1997).
[31] N. Tamura, A. A. MacDowell, R. Spolenak, B. C. Valek, J. C. Bravman, W. L. Brown, R. S. Celestre, H. A. Padmore, B. W. Batterman, and J. R. Patel, J. Synchrotron Radiat. **10**, 137 (2003).
[32] XMAS, x-ray microdiffraction analysis software, is a software suite designed specifically for the analysis of x-ray microdiffraction data collected on beamline 7.3.3 at the Advanced Light Source (ALS). The software can be freely downloaded on the ALS microdiffraction website http://xraysweb.lbl.gov/microdif/XMAS/
[33] XMAS indexing software tutorial v.1. This tutorial is available for free download from the ALS microdiffraction website http://xraysweb.lbl.gov/microdif/XMAS/
[34] B. C. Larson, N. Tamura, J. S. Chung, G. E. Ice, J. D. Budai, J. Z. Tischler, W. Yang, H. Weiland, and W. P. Lowe, Mater. Res. Soc. Symp. Proc. **590**, 247 (2000).
[35] N. Tamura, H. Padmore, and J. R. Patel, Mater. Sci. Eng., A **399**, 92 (2005).
[36] *Magnesium Alloys and Their Applications*, edited by K. U. Kainer (Wiley-VCH, Weinheim), pp. 119–124.
[37] F. Kaiser, J. Bohlen, D. Letzig, K.-U. Kainer, A. Styczynski, and C. Hartig, Adv. Eng. Mater. **5**, 891 (2003).